Chemistry, Physics and Technology of Surface. 2025. V. 16. N 4. P. 521-532

UDC 544.47+546.215+546.655 doi: 10.15407/hftp16.04.521

A.M. Hrynko [1, 2], A.V. Brichka [2], O.M. Bakalinska [1, 2], O.I. Oranska [2], H.O. Kaleniuk [2], M.T. Kartel [2]

INFLUENCE OF CALCINATION TEMPERATURE ON CATALYTIC ACTIVITY OF NANOCERIA

[1] National University of "Kyiv-Mohyla Academy"
2 Skovorody Str., Kyiv, 04070, Ukraine
[2] Chuiko Institute of Surface Chemistry of National Academy of Sciences of Ukraine
17 Oleha Mudraka Str., Kyiv, 03164, Ukraine, E-mail: bakalin2008@ukr.net

Nanoceria was synthesized by reaction of cerium nitrate deposition in an aqueous medium without stabilizers at room temperature. Nano-sized cerium oxide was dried at 20 °C and calcinated in air for 1 hour at 120, 300, 500, 800 °C. SEM images of samples demonstrated that the morphology of the obtained cerium oxide does not significantly change with the increase of the temperature of heat treatment. Electron microscopy showed that the average diameter of CeO_2 particles varies in the range of 12.4–15.9 nm. Sample element content was determined by the energy-dispersive X-ray spectrometry method. The Oxygen:Cerium elements ratio in the samples is in the range 1.7–2.1. X-Ray Diffraction method was used to determine the structural characteristics of materials. It was demonstrated that with increasing annealing temperature, the average crystallite diameter increases from 10 to 23 nm, and the degree of crystallinity changes from 60 % for Ce-20 to 100 % for Ce-800. The characteristics of the porous structure were determined based on low-temperature nitrogen adsorption/desorption isotherms. The specific surface area (BET) of the samples heated to 500 °C varies within 46–61 m^2/g. The total pore volume varies from 0.19 to 0.22 cm^3/g. After heating to 800 °C, the specific surface area and total pore volume decrease to 17 m^2/g and 0.13 cm^3/g, respectively. By TGA method was found that 5 % mass loss between 20 and 300 °C is attributed to adsorbed water, while after calcination above 300 °C, another 3.5 % mass loss refers to release from the surface of chemically bonded water molecules. The $I_{UVS\ Ce^{4+}}/I_{UVS\ Ce^{3+}}$ ratio in samples was found from UV-spectra of diffuse reflectance; it varied in the range of 1.60 to 2.08. Calcination of nanoceria samples at temperatures above 500 °C leads to the oxidation of Ce^{3+} to Ce^{4+} and reduction of nanoceria surface defects. The catalytic activity of the synthesized materials was evaluated by the determination of the reaction rate constant (k) of the H_2O_2 decomposition reaction at the different concentrations (1–10 %) at room temperature and within pH 8.0–11.0. Materials calcinated at different temperatures demonstrate maximum catalytic activity at pH 10.0, which is determined by the increase in the content of deprotonated ceranol groups on the surface of cerium oxide with an increase in the pH from 8.0 to 10.0, and the formation of insoluble Cerium compounds with a further increase in pH. The activation energy (E_a) of the reaction of hydrogen peroxide decomposition by nanoceria in the temperature range of 20–40 °C at pH 10 was determined by kinetic data. The E_a for un-annealing sample Ce-20 is 127 kJ/mol. Increasing temperature to 120 °C does not change the E_a. It was shown that the smallest value of activation energy is 77 kJ/mol for the sample calcinated at 300 °C. Heating the samples at temperatures 500 and 800 °C causes growth of E_a – to 94 and 95 kJ/mol, respectively.

We did not find correlation between degree of crystallinity, specific surface area, total pore volume, crystallite size and calcinated samples catalytic activity. The dependence of the rate constant (activity) on the calcination temperature is extreme with a maximum at 300 °C was found. A sample Ce-300, which has the highest O:Ce ratio (2.08), the largest O content (67.5 %), the lowest Ce^{4+}/Ce^{3+} ratio (0.15) among the calcinated samples, and therefore the largest number of surface defects exhibits the highest catalytic activity and has the lowest activation energy for the hydrogen peroxide decomposition reaction. Presumably, when heating CeO_2 samples, some parallel processes occur. Changes in the values of structural parameters either have no effect or are insignificant and also do not affect the catalytic activity of nanoceria. Desorption of physically adsorbed water, which inactivates the catalytic centers, leads to an increase in catalytic activity of the material. In addition, destruction of ceranol groups on the surface of cerium oxide with loss of oxygen and oxidation of Ce^{3+} to Ce^{4+} reduces catalytic activity.

***Keywords**: cerium oxide nanoparticles, calcination, catalytic activity, hydrogen peroxide decomposition, activation energy*

INTRODUCTION

Nanosized cerium oxide have fascinated broad interest from numerous researches due to its promising applications in such fields as chemistry, biology, physics and materials science [1]. Nanoceria and cerium-containing materials are already used or proposed for the wide technological significance, such as ultraviolet

(UV) absorbents [2], catalysts [3], polishing agents [4], gas sensors [5], solid oxide fuel cells [6], diesel fuel additives [7]. In biomedical application cerium oxide nanoparticles has high perspective for oxidative stress-related diseases treatment [8]. Nanoceria demonstrated anti-inflammatory and antimicrobial activity [9], anticancer activity [10], anti-diabetic property [11], cardioprotective effects [12], and promising for neurodegenerative diseases, for example, Alzheimer's and Parkinson's diseases treatment [13].

Wide interest in nanoscale cerium oxide is associated with its unique structure and unusual redox properties. Cerium is a lanthanide with an atomic number of 58, can exist in two oxidation forms of Ce^{3+} and Ce^{4+} and in bulk, it forms two oxides – Ce_2O_3 and CeO_2. At the nanoscale, cerium oxide lattice has a cubic fluorite structure and both Ce^{3+} and Ce^{4+} can coexist on the surface [14]. Redox cycling between Ce^{3+} and Ce^{4+} ions on the surface of cerium oxide nanoparticles leads to the formation of oxygen vacancies on the nanoceria surfaces [15]. The ratio of Ce^{4+}/Ce^{3+} sites on the nanoceria surface is a measure of the concentration of these oxygen vacancies concentrations [16]. These oxygen vacancies are essentially surface defects, the number of which increases with decreasing particle size. When the particle becomes smaller – the nanoceria lattice expands and the ability to absorb and release oxygen increases. The ratio of Ce^{4+}/Ce^{3+} sites on the surface is strongly correlated with antioxidant enzyme-mimetic activity [17]. Nanoceria acts like the natural ferments - catalase (CAT) and superoxide dismutase (SOD) in scavenging reactive oxygen species (ROS) such as hydrogen peroxide and superoxide radicals in the cell and animal models [18].

Redox properties and catalytic activity of cerium oxide nanomaterials are mainly dependent on physicochemical properties such as size, agglomeration, morphology, surface chemistry, and valence of the structure [19]. To obtain materials with various characteristics, several methods have been proposed including precipitation [20], hydrothermal [21], microemulsion [22], sol-gel [23], solvothermal [24], combustion [25], green synthesis [26]. Synthesis conditions such as pH [27], temperature [28], time, stabilizing agents [29], concentration and nature of the precursors [30] may affect significantly the properties of the final product. Studies have suggested that calcination leads to an increase in degree in crystallinity and particle size [31]. With increasing particle size, the lattice parameter decreases and the lower oxygen vacancies content are presented on the surface [32]. However, there are only several studies about the influence of calcination temperature on the catalytic activity of nanoceria.

The aim of this work is the preparation of nanoceria samples; calcination it at different temperatures; characterization its properties; elucidation of the effect of nanoceria calcination on the catalytic activity and on the effective activation energy of the reaction of the hydrogen decomposition by synthesized nanoceria samples.

MATERIALS AND METHODS

Nanoceria was synthesized by reaction of cerium nitrate deposition in an aqueous medium without stabilizers at room temperature according to the reaction:

$$4Ce(NO_3)_3 + 12NaOH + O_2 = \\ = 4CeO_2 + 12NaNO_3 + 6H_2O.$$

The cerium oxide nanoparticles were dried at 20 °C and calcinated in muffle furnace SNOL-1.8 for 1 hour at 120, 300, 500, 800 °C (Ce-20, Ce-120, Ce-300, Ce-500, Ce-800). The morphology of the synthesized materials was studied by scanning electron microscopy. Sample element content was determined by the energy-dispersive X-ray spectrometry method on X-Max by Oxford Instruments. This method is based on the registration and analysis of the energy spectra of characteristic X-rays. The XRD analysis was performed using a DRON-4-07 diffractometer, with nickel-filtered CuK_α radiation in the range of $2\theta = 10$ to 85° for phase identification. UV-Vis spectra were obtained using a Shimadzu UV–VIS–NIR spectrophotometer UV-3600 in the 220–800 nm range with an instrument uncertainty of ± 1 nm. The FTIR spectra of ceria nanoparticles were recorded using a Thermo Nicolet Nexus FT-IR spectrometer in 5000–400 cm^{-1} diapason at room temperature. The catalytic activity of the nanoceria and the effective activation energy of the reaction was determined in a model reaction of the decomposition of hydrogen peroxide. The rate of the decomposition of hydrogen peroxide was monitored by measuring the volume of oxygen gas evolved as a function of time. A volumetric method was used to study the kinetics of the

decomposition of hydrogen peroxide. The initial concentration of hydrogen peroxide in solutions was determined by permanganometry. The experiment was conducted for 30 min with a constant stirring of the reaction mixture having a total volume of 25 mL. The volume of oxygen released was fixed with a precision of 0.02 mL. The catalytic activity of the materials was evaluated by the determination of the reaction rate constant (k, s^{-1}). The maximum reaction rate was determined from the kinetic data of the decomposition of substrate solutions with a concentration of 1–10 % in the pH range of 8.0 to 11.0 (borate buffer) by the optimum catalyst weight. The activation energy of the reaction was determined based on the dependence of the reaction rate constant on the reciprocal temperature. The experiments were carried out at temperatures of 20, 25, 30, 35, 40 °C (pH 10.0).

RESULTS AND DISCUSSION

Both the morphology and structural characteristics of the samples influence their catalytic activity.

By SEM analysis it was showed that the morphology of the cerium oxide does not change significantly with the increase of the temperature of heat treatment (Fig. 1).

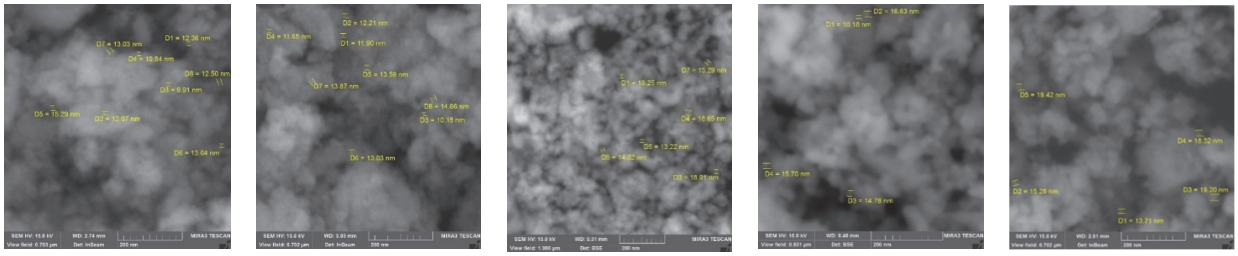

a *b* *c* *d* *e*

Fig. 1. SEM images of nanoceria samples calcinated at (*a*) 20 °C, (*b*) 120 °C, (*c*) 300 °C, (*d*) 500 °C, (*e*) 800 °C for 1 hour

SEM images of the studied samples allowed to calculate the average particle size (Table 1). Increasing the processing temperature leads to the formation of larger particles due to agglomeration and enhanced crystallite growth. If the average diameter of nanosized cerium oxide particles after drying at 20 °C is 12.4 nm, then calcination of samples to a temperature of 800 °C leads to an increase in the average size of CeO_2 particles to 15.9 nm.

The Energy Dispersive X-ray (EDX) microanalysis for the identification of elements and their weight percentages was used (Table 1). It has been demonstrated that the weight percentage of Ce and O changes as the calcination temperature increases. The O:Ce elements ratio in the samples was in the range 1.60–2.08. This ratio was highest for the sample calcined at 300 °C. The O:Ce elements ratio raised from 1.86 to 2.08 and after decrease to 1.60. After calcination at 800 °C the O:Ce element ratio raised to 1.69.

Table 1. The content of elements in nano-sized cerium oxide samples according to the EDX analysis

Sample treatment temperature,	Particle size, nm	O, %	Ce, %	O:Ce
20	12.4±2.7	65.0	35.0	1.86
120	12.6±2.2	66.3	33.7	1.97
300	15. 5±2.9	67.5	32.5	2.08
500	10.5±1.3	61.6	38.4	1.60
800	15.9±4.6	62.8	37.2	1.69

Two parallel processes have occurred during the calcination of the samples. One process was the destruction of the hydroxyl groups on the cerium oxide surface with the loss of oxygen. And the second one was the oxygen absorption by air filling the oxygen vacancies of cerium oxide.

Predominance of one process from the another causes growth, and then a decrease in the oxygen content with increasing calcination temperature.

To measure the mass loss percentage and derivative mass loss thermogravimetric analysis was used (Fig. 2). Defined from the TGA curve weight loss is comprised of several stages, including physical water desorption and chemically bonded water molecules desorption. Mass loss of 5 % between 20 and 300 °C is attributed to adsorbed water, while after calcination above 300 °C, another 3.5 % mass loss refers to release from the surface of chemically bonded water molecules.

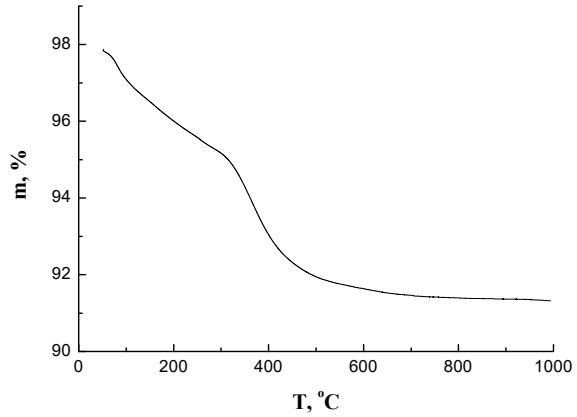

Fig. 2. TGA curve of a sample of nanoceria, dried at 20 °C

The parameters of the porous structure of the synthesized materials were studied by low temperature nitrogen adsorption-desorption method (Table 2, Fig. 3). It is shown that the porosity structure of all studied samples is similar and determined during the synthesis of nanosized cerium oxide. According to the classification of the International Union of Pure and Applied Chemistry, the adsorption curve belongs to the type IVa adsorption isotherm, with a distinct hysteresis loop, indicating capillary condensation in the mesopores. The profile of the hysteresis loop can be attributed to the H1 type. It is believed that the type of hysteresis H1 is associated with the a corpuscular porous structure formed by particles of similar size with uniform packing.

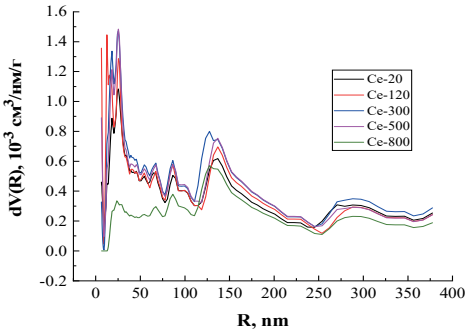

Fig. 3. Pore size distribution of investigated CeO_2 samples (DFT)

The specific surface area and pore size of the synthesized material are important factors in determining the catalytic activity. The BET specific surface areas (S_{BET}), total pore volumes (V_P) and DFT pore sizes are calculated from the isotherms (Table 2). The samples contain mesopores with a radius in the range of 13–25 nm and macropores with a radius in the range of 125–150 nm. Increasing the heating temperature of the CeO_2 sample to 800 °C leads to a significant decrease in mesopores. The specific surface area of the samples heated to 500 °C, determined by BET, varies within 46–61 m^2/g. The total pore volume determined at the maximum value of p/p_s varies from 0.19 to 0.22 cm^3/g. After heating to 800 °C, the specific

surface area and total pore volume decrease to 17 and 0.13 cm^3/g, respectively, due to a decrease in the mesopore content due to thermal transformations of the sample.

XRD method was used to determine the structural characteristics of cerium oxide materials. Fig. 4 depicts the X-ray diffraction spectra of CeO_2 nanoparticles at different calcination temperatures for 1 hour. The average crystallite size of the cerium oxide nanoparticles calcinated at different temperatures was determined by the Scherrer equation [33]:

$$D = \frac{K\lambda}{\beta \cos\theta}$$

where D represents the average crystallite size of the synthesized cerium oxide, K is a dimensionless shape factor, with a value 0.89, λ is the X-ray wavelength of Cu K_α , β is the full width of the peak measured at half maximum intensity (FWHM) and θ is the Bragg angle of the peak.

Table 2. Structural and sorption characteristics of calcinated nanoceria

Material	S_{BET}, m^2/g	V_P, cm^3/g	R_{pore}, nm (DFT)	Average size of crystallites, nm	The degree of crystallinity φ, %
Ce-20	46	0.19	25	10	60
Ce-120	61	0.19	13	10	80
Ce-300	54	0.22	25	10	80
Ce-500	57	0.20	25	12	90
Ce-800	17	0.13	128	23	100

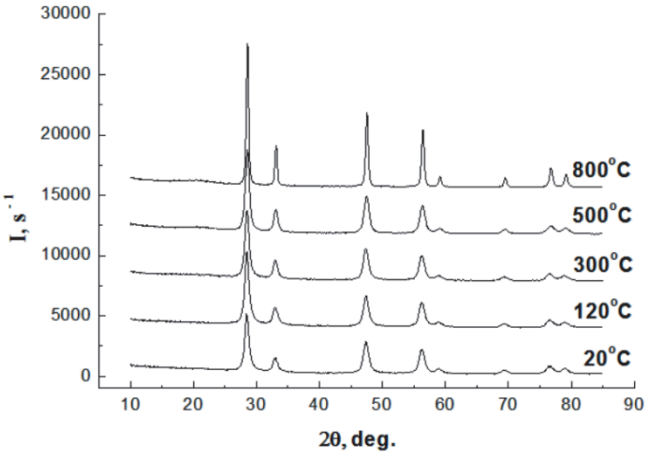

Fig. 4. XRD spectra of CeO_2 nanoparticles, calcined at different temperatures

The degree of crystallinity was calculated based on the linear dependence of the integral intensity of the diffraction peaks on the content of the critical phase in the sample. In a two-phase system (amorphous and crystalline CeO_2) with the same mass absorption coefficients, the degree of crystallinity is recorded as the ratio of the integral peak intensities of the sample to be studied and fully crystalline sample (we took CeO_2, which is calcinated at 800 °C as a fully crystalline):

$$\varphi = \frac{I_{CeO_2}}{I_{CeO_2(800)}} \times 100\%.$$

The average size of the crystallites and the degree of crystallinity of CeO_2 were determined by the diffraction peak (111) at 2θ = 28.45 deg. Table 3 presents the structural characteristics of the samples.

With increasing annealing temperature, the average size of crystallites and the degree of crystallinity increases. Thus, for the sample dried at 20 °C the degree of crystallinity was 60 % and the average crystallite size of 10 nm, while for the sample, calcinated at 800 °C, the value of these parameters was increased to100 % and 23 nm, respectively (Table 2).

FTIR spectroscopy was used to determine the effect of temperature treatment of cerium oxide nanoparticles on their chemical bonds. Fig. 5*a* shows the IR spectra in the diffuse reflection mode, and Fig. 5*b* shows the spectroscopic visualization in the disturbed total internal reflection (DTR) mode of unannealed and annealed at different temperatures samples of nanosized cerium oxide.

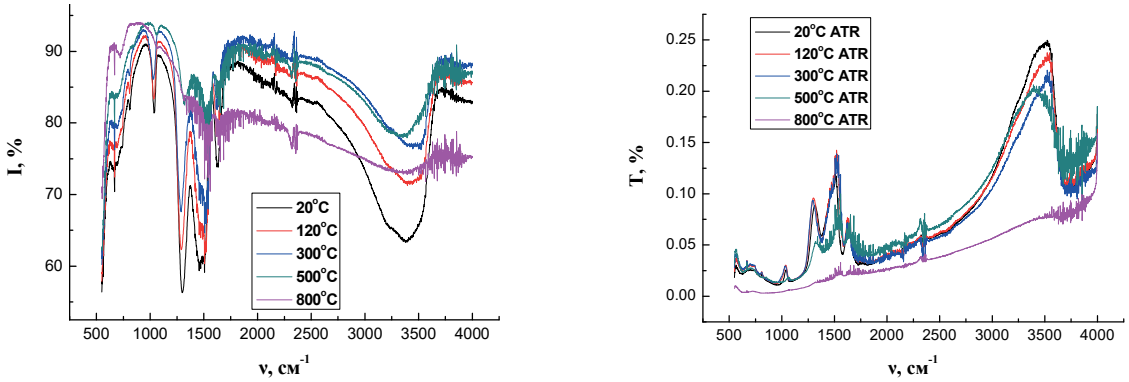

a *б*

Fig. 5. IR spectra of samples Ce-20, Ce-120, Ce-300, Ce-500, Ce-800 in the diffuse reflection (*a*) and disturbed total internal reflection (*b*) modes

The DTR spectra are almost identical to conventional absorption spectra, the difference is that the bands in the long-wavelength region are more intense than in the short-wavelength region compared to the transmission spectrum of the substance (Fig. 5 *b*). In the spectra of all studied samples, the presence of CeO_2 is confirmed by an absorption band of about 500 cm^{-1}, which corresponds to vibrations of Ce-O bonds. In [34], the authors observed the appearance of new peaks at 1020, 1050, and 1100 cm^{-1}, corresponding to the initial nanosized cerium oxide and calcinated at 100 and 200 °C, respectively, and suggested that these peaks are the result of the interaction of Ce atoms with CO_2 in the atmosphere, which leads to oscillations of Ce-O-C bonds. In the studied samples, such peaks are observed at ~1060 cm^{-1}, with the absorption intensity increasing with increasing sample processing temperature. The bands at 1300 cm^{-1} correspond to deformation vibrations of water. The bands at ~1625 cm^{-1} arise from vibrations of the H-O-H bond, which is overlapped by a band corresponding to O-C-O stretching (the intensity of which changes after annealing of the samples). The broad band at 3450 cm^{-1} corresponds to stretching vibrations of the O-H bonds of hydroxyl groups.

The catalytic behavior of cerium oxide nanoparticles is determined by the surface defectivity, namely the presence of oxygen vacancies on the surface of nanosized cerium oxide. The defectivity is measured by the ratio of Ce^{4+}/Ce^{3+} ions, which was determined from UV-Vis diffuse reflectance spectra (Table 3, Fig. 7 *a*). Increasing temperature of processing of samples leads to a decrease in the number of surface defects due to particle aggregation and a decrease in their specific surface area.

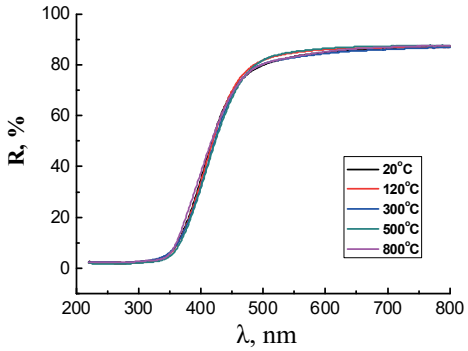

Fig. 6. UV-Vis diffuse reflection spectra of cerium oxide nanoparticles calcinated at different temperatures

The Ce^{4+}/Ce^{3+} ratio was defined as the ratio of the integral signal intensities (Fig. 7 *a*). Mathematical processing of UV-Vis spectra of nanocomposites allowed decomposing the peaks of cerium oxide into two components, corresponding to cerium in different valence states: Ce^{3+} and Ce^{4+} as indicated elsewhere [35]. Even though the lower wavelength limit is

220 nm, extrapolating the experimental data to the unexplored region of the spectrum and its deconvolution into the sum of Gaussian functions, it is possible to distinguish a peak, which we refer to Ce^{4+}. An increase in the content of cerium oxide and, accordingly, in nanoparticle diameter results in an increase in the relative content of Ce^{4+} and a decrease in the relative content of Ce^{3+} (Table 3).

In the UV-Vis spectrum of cerium nanocomposites, the bands with a maximum located near 207–223 nm are ascribed to Ce^{4+} and the bands with maximums around 310–337 nm to Ce^{3+}. This analysis of UV-Vis spectra is not quantitative; it only allows us to estimate the relative content of the multivalent state of cerium oxide.

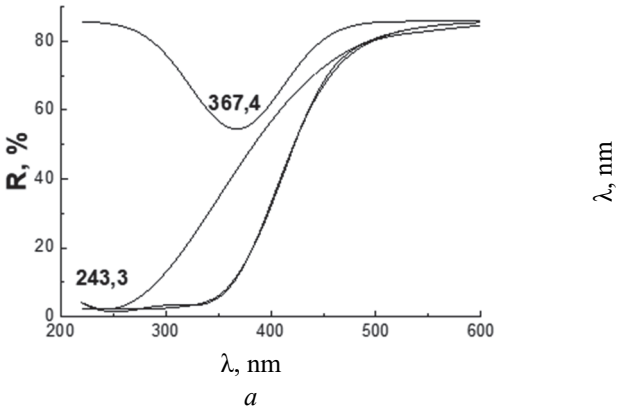

a *b*

Fig. 7. Deconvolution of UV-Vis diffuse reflectance spectra of Ce-300 sample (*a*), dependence of the Ce^{3+} and Ce^{4+} peaks maximum position in the UV-Vis spectra on calcination temperature (*b*)

The maximum of the band of Ce^{3+} shifts to a longer wavelength with an increase in the treatment temperature of the nanoceria to 300 °C. And with a further increase in the calcination temperature to 800 °C, the band of Ce^{3+} shifts to shorter wavelengths. The position of the maximum of the band of Ce^{4+} shifts to the short-wavelength region (hypsochromic shift) (Fig. 7 *b*). Calcination of cerium oxide nanoparticles promotes the formation of larger crystalline particles on the surface of which Ce^{4+} ions predominate [36]. Calcination of nanoceria samples at temperatures above 500 °C leads to the oxidation of Ce^{3+} to Ce^{4+} and to an increase in the ratio $I_{UVS\ Ce^{4+}}/I_{UVS\ Ce^{3+}}$ (Fig. 8).

The catalytic activity of the synthesized materials was evaluated by the determination of the reaction rate constant (k) of the H_2O_2 decomposition reaction at the different concentrations (1–10 %) at room temperature and within pH 8.0–11.0 (Fig. 9). Materials calcinated at different temperatures demonstrate maximum catalytic activity at pH 10.0, which is determined by the increase in the content of deprotonated ceranol (≡Ce-O-) groups on the surface of cerium oxide with an increase in the pH from 8.0 to 10.0, and the formation of insoluble Cerium compounds with a further increase in pH. Nanoceria samples exhibit maximum catalytic activity at pH 10.0. The sample calcinated at 300 °C possessed the best catalytic activity (Table 3). This is due to the fact that heating under this temperature physically adsorbed water molecules are desorbed and catalytic centers became active. Samples heating at higher temperature leads to release from the surface of chemically bonded water molecules and to the oxidation of Ce^{3+} to Ce^{4+}. As a result, a decrease in the catalytic activity takes place.

The activation energy of the H_2O_2 decomposition reaction by the synthesized samples was determined from the dependence of the reaction rate constants on temperature in the temperature range of 20–40 °C at pH 10.0 (Fig. 10). The activation energy for un-annealing sample Ce-20 is 127 kJ/mol. Increasing temperature to 120 °C does not change the E_a. It has been shown that the smallest value of activation energy is 77 kJ/mol for the sample, calcinated at 300 °C. Heating the samples at higher temperatures – 500 and 800 °C causes growth of E_a to 94 and 95 kJ/mol, respectively (Table 3).

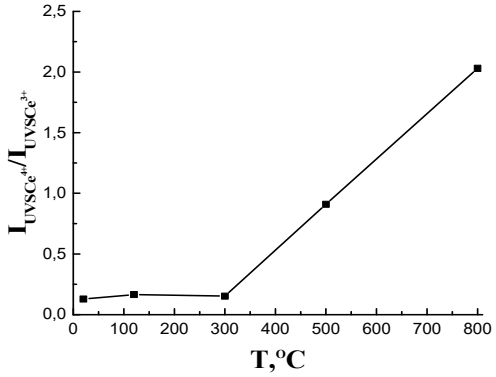

Fig. 8. Dependence of the composition of the integral intensities of CeO_2 peaks on the calcination temperature

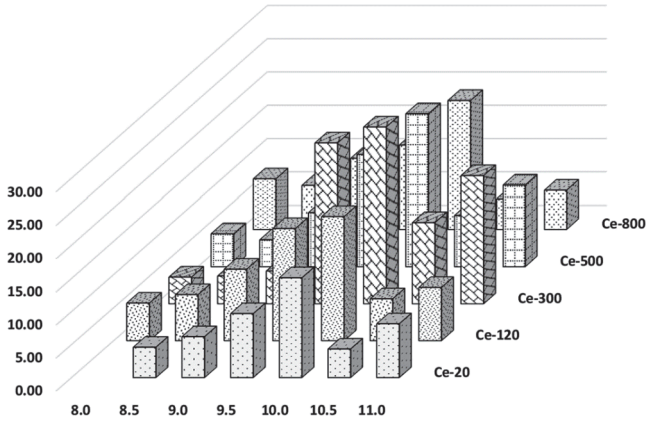

Fig. 9. Dependence of samples catalytic activity (k, s^{-1}) on pH

Table 3. Dependence of structural characteristics, the content of elements, catalytic activity, and activation energy of the reaction on the calcination temperature

Sample treatment temperature, T °C	Ce^{4+}/Ce^{3+}	Activity, k, s^{-1}	E_a, kJ/mol
20	0.13	15.1	127
120	0.17	18.7	127
300	0.15	26.5	77
500	0.91	22.9	94
800	2.08	19.3	95

The particles processing temperature determines their physical and chemical characteristics, which, in turn, influences the catalytic activity of the materials and the effective activation energy of the hydrogen peroxide decomposition reaction. It was found that the calcination temperature does not change the morphology of CeO_2 particles. The average size of crystallites varies, but does not correlate with activity, since the Ce-20, Ce-120 and Ce-300 samples have the same crystallite sizes, but exhibit different activity. The degree of crystallinity also does not correlate with activity, since the samples with the highest degree of crystallinity are not the most active. Calcination up to 500 °C practically does not change the surface area and pore volume. Calcination at 800 °C reduces the surface area and pore volume. We did not find any correlation between the change in the degree of crystallinity and structural parameters of the CeO_2 samples as a result of calcination and their catalytic activity.

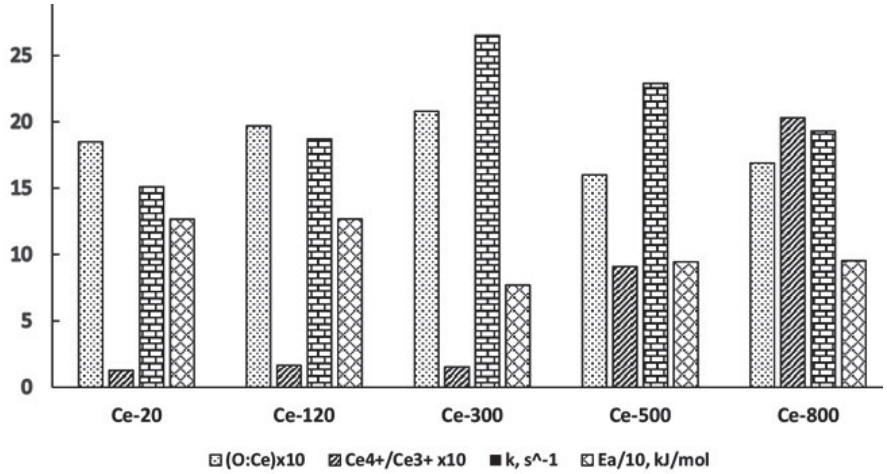

Fig. 10. O:Ce ratio, Ce^{4+}/Ce^{3+} ratio, catalytic activity (k, s^{-1}), activation energy of the hydrogen peroxide decomposition reaction at pH 10.0 for calcinated nanosized CeO_2 samples

Fig. 10 presents O:Ce ratio, Ce^{4+}/Ce^{3+} ratio and the catalytic activity (k, s^{-1}) and the effective activation energy of the hydrogen peroxide decomposition reaction determined at pH 10. The dependence of the rate constant (activity) on the calcination temperature is extreme with a maximum at 300 °C. For all samples, an inverse proportionality between the values of k and E_a is observed. The Ce-300 sample has the largest rate constant and the smallest activation energy of the hydrogen peroxide decomposition reaction. The sample is characterized by the largest O:Ce ratio (2.08) - the largest O content (67.5 %) and the smallest Ce^{4+}/Ce^{3+} ratio (0.15), and therefore a larger number of surface defects. It can be assumed that during the calcination of CeO_2 samples to 300 ℃, desorption of physically adsorbed water which inactivates the catalytic centers occurs. At the same time, the surface defectivity of the samples Ce-120 and Ce-300 - the ratio Ce^{4+}/Ce^{3+} decreases slightly. Therefore, the activity of the samples increases. With a further increase in the treatment temperature, the physically adsorbed water is release of the ratio O:Ce decreases and the oxidation of Ce^{3+} to Ce^{4+} occurs, which reduces the surface defectivity.

CONCLUSION

A number of samples of nanosized cerium oxide were synthesized by the chemical precipitation method without stabilizers at room temperature from aqueous solutions of cerium nitrate with subsequent heat treatment at 120, 300, 500, 800 °C. Their physicochemical properties were characterized, and their catalytic activity in a model reaction of hydrogen peroxide decomposition was studied. The activation energy of the H_2O_2 decomposition reaction by the synthesized samples was determined from the dependence of the reaction rate constants on temperature in the temperature range of 20–40 °C at pH 10.0. Materials calcinated at different temperatures demonstrate maximum catalytic activity at pH 10.0, which is determined by the increase in the content of deprotonated ceranol (≡Ce-O-) groups on the surface of cerium oxide with an increase in the pH from 8.0 to 10.0, and the formation of insoluble Cerium compounds with a further increase in pH. Increasing the calcination temperature of CeO_2 samples increases the degree of crystallinity, but does not correlate with samples activity. Increasing the calcination temperature to 500 ℃ has little effect on the change in the specific surface area, total pore volume, and crystallite size. Heating to 800 C reduces the structural parameters. We did not find correlation between those parameters and samples catalytic activity. The dependence of the rate constant (activity) on the calcination temperature is extreme with a maximum at 300 °C was found. Sample Ce-300, which has the highest O:Ce ratio (2.08), the largest O content (67.5 %), the lowest Ce^{4+}/Ce^{3+} ratio among the calcinated samples (0.15), and therefore the largest number of surface defects exhibits the highest catalytic activity and has the lowest activation energy for the hydrogen peroxide decomposition reaction. Presumably, when heating CeO_2 samples, some parallel processes occur - desorption of physically adsorbed water,

which inactivates the catalytic centers. This process leads to an increase in catalytic activity of the material. In addition, destruction of ceranol groups on the surface of cerium oxide with loss of oxygen and oxidation of Ce^{3+} to Ce^{4+}, which reduces catalytic activity.

Вплив темпераратури прожарювання на каталітичну активність нанооксиду церію

А.М. Гринько, А.В. Бричка, О.М. Бакалінська, О.І. Оранська, Н.О. Каленюк, М.Т. Картель

Національний університет «Києво-Могилянська академія»
вул. Сковороди, 2, Київ, 04070, Україна
Інститут хімії поверхні ім. О.О. Чуйка Національної академії наук України
вул. Олега Мудрака, 17, Київ, 03164, Україна, alinagrinko2@gmail.com

Нанорозмірний оксид церію було синтезований реакцією осадження нітрату церію у водному середовищі без стабілізаторів за кімнатної температури. Одержані частинки оксиду церію сушили при 20 °C та прожарювали на повітрі протягом 1 години при 120, 300, 500, 800 °C. СЕМ зображення зразків показали, що морфологія отриманого оксиду церію істотно не змінюється зі збільшенням температури обробки. За даними електронної мікроскопії середній діаметр частинок CeO_2 знаходиться у межах 12.4–15.9 нм. Вміст елементів у зразку визначали методом енергодисперсійної рентгенівської спектрометрії. Співвідношення O:Ce у зразках знаходилось в діапазоні 1.7–2.1. Для визначення структурних характеристик матеріалів було використано метод рентгенівської дифракції. Було встановлено, що зі збільшенням температури відпалу середній діаметр кристалітів збільшується від 10 до 23 нм, а ступінь кристалічності змінюється від 60 % для Ce-20 до 100 % для Ce-800. Характеристики пористої структури визначали за низькотемпературними ізотермами адсорбції/десорбції азоту. Питома поверхня (BET) зразків, прожарених до 500 °C змінюється у межах від 46 до 61 $м^2/г$. Загальний об'єм пор змінюється від 0.19 до 0.22 $см^3/г$. Прожарювання при 800 °C призводить до зменшення питомої поверхні та загального об'єму пор до 17 $м^2/г$ та 0.13 $см^3/г$ відповідно. Методом TGA встановлено, що 5 % втрати маси між 20 і 300 °C пояснюється втратою адсорбованої води, тоді як після прожарювання вище 300 °C, втрата ще 3.5 % маси - стосується вивільнення з поверхні хімічно зв'язаних молекул води. Співвідношення $I_{UVS\ Ce^{4+}}/I_{UVS\ Ce^{3+}}$ у зразках оцінювали за УФ-спектрами дифузного відбиття; воно змінювалося в діапазоні від 1.60 до 2.08. Прожарювання зразків нанооксиду церію за температур вище 500 °C призводить до окиснення Ce^{3+} до Ce^{4+} та зменшення дефектності поверхні нанооксиду церію. Каталітичну активність синтезованих матеріалів оцінювали визначенням констант швидкості реакції (k) розкладання H_2O_2 при різних концентраціях (1–10 %) за кімнатної температури та в діапазоні pH 8.0–11.0. Матеріали, прожарені за різних температур, демонструють максимальну каталітичну активність при pH 10.0, що визначається збільшенням вмісту депротонованих церанольних груп на поверхні оксиду церію зі збільшенням pH від 8.0 до 10.0, та зменшенням активності при утворенні нерозчинних сполук церію при подальшому підвищенні pH. Енергію активації (E_a) реакції розкладання пероксиду водню зразками нанооксиду церію в діапазоні температур 20–40 °C при pH 10 визначали за кінетичними даними. E_a для невідпаленого зразку Ce-20 становить 127 кДж/моль. Збільшення температури до 120 °C не змінює E_a. Було показано, що найменше значення енергії активації становить 77 кДж/моль для зразка, прожареного при 300 °C. Нагрівання зразків до температур 500 та 800 °C призводить до зростання E_a до 94 та 95 кДж/моль відповідно.

Ми не виявили кореляції між ступенем кристалічності, питомою поверхнею, загальним об'ємом пор, розміром кристалітів та каталітичною активністю прожарених зразків. Встановлено екстремальну залежність константи швидкості (активності) від температури прожарювання з максимумом при 300 °C. Зразок Ce-300, який має найвище співвідношення O:Ce (2.08), найбільший вміст O (67.5 %), найнижче співвідношення Ce^{4+}/Ce^{3+} (0.15) серед прожарених зразків, а отже, найбільшу кількість поверхневих дефектів, виявляє найвищу каталітичну активність та має найнижчу енергію активації реакції розкладання пероксиду водню. Ймовірно, при нагріванні зразків CeO_2 відбувається декілька паралельних процесів. Зміни значень структурних параметрів або не впливають, і на каталітичну активність нанооксиду церію або є незначними. Відбувається десорбція фізично адсорбованої води, яка інактивує каталітичні центри. Цей процес приводить до підвищення каталітичної активності матеріалу. Крім того, відбувається відщеплення церанольних груп з поверхні оксиду церію з втратою кисню та окиснення Ce^{3+} до Ce^{4+}, що знижує каталітичну активність.

***Ключові слова**: наночастинки оксиду церію, кальцинація, каталітична активність, розкладання пероксиду водню, енергія активації*

REFERENCES

1. Seal S., Jeyaranjan A., Neal C.J., Kumar U., Selvan T., Sayle D.C. Engineered defects in cerium oxides: tuning chemical reactivity for biomedical, environmental, & energy applications. *Nanoscale*. 2020. **12**(13): 6879.
2. Miri A., Sarani M., Khatami M. Nickel-doped cerium oxide nanoparticles: biosynthesis, cytotoxicity and UV protection studies. *RSC Advances*. 2020. **10**(7): 3967.
3. Zhang M., Zhang S., Oi Z., Xie M., Qu Y. Recent advancements in CeO_2-enabled liquid acid/base catalysis. *Catal. Sci. Technol.* 2024. **14**(2): 225.
4. He Q. Experimental study on polishing performance of CeO_2 and nano-SiO_2 mixed abrasive. *Appl. Nanosci*. 2018. **8**: 163.
5. Nithyavathy N., Rajendran V., John Berchmans L., Maaza M., Krithika S., Arunmetha S. Gas sensing behaviour of cerium oxide and magnesium aluminate composites. *Bull. Mater. Sci.* 2017. **40**(4): 667.
6. Omar S. Doped ceria for solid oxide fuel cells. *Intech Open*. 2019. **4**: 43.
7. Dale J.G., Cox S.S., Vance M.E., Marr L.C., Hochella M.F. Transformation of cerium oxide nanoparticles from a diesel fuel additive during combustion in a diesel engine. *Environ. Sci. Technol.* 2017. **51**(4): 1973.
8. Kim Y.G., Lee Y., Lee N., Soh M., Kim D., Hyeon T. Ceria-Based Therapeutic Antioxidants for Biomedical Applications. *Adv. Mater.* 2024. **36**(10): 2210819.
9. Gomes-da-Silva N.C., Correa L.B., Gonzalez M.M., Franca A.R.S., Alencar L.M.R., Rosas E.C., Ricci-Junior E., Aguiar T.K.B., Souza P.F.N., Santos-Oliveira R. Nanoceria Anti-inflammatory and Antimicrobial Nanodrug: Cellular and Molecular Mechanism of Action. *Curr. Med. Chem*. 2025. **32**(5): 1017.
10. Tang J.L.Y., Moonshi S.S., Ta H.T. Nanoceria: an innovative strategy for cancer treatment. *Cell. Mol. Life Sci.* 2023. **80**(2): 46.
11. Chen S., Wang Y., Bao S. Yao L., Fu X., Yu Y., Lyu H., Pang H., Guo S., Zhang H., Zhou P., Zhou Y. Cerium oxide nanoparticles in wound care: a review of mechanisms and therapeutic applications. *Front. Bioeng. Biotechnol.* 2024. **12**: 1404651.
12. Kumari P., Saifi M.A., Khurana A., Godugu C. Cardioprotective effects of nanoceria in a murine model of cardiac remodeling. *J. Trace Elem. Med. Biol.* 2018. **50**: 198.
13. Monroy-Ramirez H.C., Salto-Sevilla J., Arceo-Orozco S., Caloca-Camarena F., Flores-Pena R., Lopez-Mena E., Galicia-Moreno M., Armendariz-Borunda J. Cerium oxide nanoparticles: a promising nanotherapy approach for chronic degenerative diseases. *J. Mater. Sci.: Mater. Eng.* 2025. **20**: 69.
14. Charbgoo F., Bin Ahmad M., Darroudi M. Cerium oxide nanoparticles: green synthesis and biological applications. *Int. J. Nanomedicine*. 2017. **12**: 1401.
15. Mehmood R., Mofarah S.S., Chen W.-F., Koshy P., Sorrell C.C. Surface, Subsurface, and Bulk Oxygen Vacancies Quantified by Decoupling and Deconvolution of the Defect Structure of Redox-Active Nanoceria. *Inorg. Chem*. 2019. **58**(9): 6016.
16. Vinothkumar G., Arunkumar P., Mahesh A., Dhayalan A., Suresh Babu K. Size- and defect-controlled anti-oxidant enzyme mimetic and radical scavenging properties of cerium oxide nanoparticles. *New J. Chem.* 2018. **42**(23): 18810.
17. Baldim V, Bedioui F., Mignet N., Margaill I., Berret J.-F. The enzyme-like catalytic activity of cerium oxide nanoparticles and its dependency on Ce^{3+} surface area concentration. *Nanoscale*. 2018. **10**(15): 6971.
18. Othman A., Gowda A., Andreescu D., Hassan M.H., Babu S.V., Seo J., Andreescu S. Two decades of ceria nanoparticle research: structure, properties and emerging applications. *Mater. Horiz.* 2024. **11**: 3213.
19. Thakur N., Manna P., Das J. Synthesis and biomedical applications of nanoceria, a redox active nanoparticle. *J. Nanobiotechnol*. 2019. **17**(1): 84.
20. Liu Z., Li X., Mayyas M., Koshy P., Hart J.N., Sorrell C.C. Growth mechanism of ceria nanorods by precipitation at room temperature and morphology-dependent photocatalytic performance. *CrystEngComm.* 2017. **19**(32): 4766.
21. Trenque I., Magnano G.C., Bolzinger M.A., Roiban L., Chaput F., Pitault I., Briançon S., Devers T., Masenelli-Varlot K., Bugnet M., Amans D. Shape-selective synthesis of nanoceria for degradation of paraoxon as a chemical warfare simulant. *Phys. Chem. Chem. Phys.* 2019. **21(**10): 5455.
22. Shlapa Y., Sarnatskaya V., Timashkov I., Yushko L., Antal I., Gerashchenko B., Nychyporenko I., Belous A., Nikolaev V., Timko M. Synthesis of CeO_2 nanoparticles by precipitation in reversal microemulsions and their physical–chemical and biological properties. *Appl. Phys. A*. 2019. **125**: 412.
23. Sakthiraj K., Karthikeyan B. Synthesis and characterization of cerium oxide nanoparticles using different solvents for electrochemical applications. *Appl. Phys. A*. 2020. **126**(1): 52.
24. Zadehnazari A. Chemical synthesis strategies for metal oxide nanoparticles: a comprehensive review. *Inorg. Nano-Metal Chem.* 2024. **55**(6): 734.

25. Ghahramani Z., Arabi A.M., Shafiee Afarani M., Mahdavian M. Solution combustion synthesis of cerium oxide nanoparticles as corrosion inhibitor. *Int. J. Appl. Ceram. Technol.* 2019. **17**(3): 1514.
26. Strieder C.M., Macuvele D.L.P., Soares C., Padoin N., Riella H.G. Plant-mediated green synthesis of cerium oxide nanoparticles: A critical perspective of some unclear issues. *J. Mater. Res. Technol.* 2024. **30**: 6376.
27. Ramachandran M., Subadevi R., Sivakumar M. Role of pH on synthesis and characterization of cerium oxide (CeO_2) nano particles by modified co-precipitation method. *Vacuum Volume.* 2019. **161**: 220.
28. Chen B.-H., Stephen Inbaraj B. Various physicochemical and surface properties controlling the bioactivity of cerium oxide nanoparticles. *Crit. Rev. Biotechnol.* 2018. **38**(7): 1003.
29. Nyoka M., Choonara Y.E., Kumar P., Kondiah P.D., Pillay V. Synthesis of cerium oxide nanoparticles using various methods: implications for biomedical applications. *Nanomaterials*. 2020. **10**(2): 242.
30. Trenque I., Magnano G.C., Bolzinger M.A., Roiban L., Chaput F., Pitault I., Briançon S., Devers T., Masenelli-Varlot K., Bugnet M., Amans D. Shape-selective synthesis of nanoceria for degradation of paraoxon as a chemical warfare simulant. *Phys. Chem. Chem. Phys*. 2019. **21**(10): 5455.
31. Kasi G., Stalin N., Rachtanapun P., Jantanasakulwong K., Halder J.N., Phongthai S., Worajittiphon P., Seo J., Thanakkasaranee S. Effect of Calcination Temperatures on Crystallite Size, Particle Size, and Antimicrobial Activity of Synthesized MgO and Its Cytotoxicity. *Int. J. Mol. Sci.* 2025. **26**(10): 4868.
32. Zhan F., Wen G., Li R., Feng C., Liu Yi., Liu Ya., Zhu M., Zheng Y., Zhao Y., La P. A comprehensive review of oxygen vacancy modified photocatalysts: synthesis, characterization, and applications. *Phys. Chem. Chem. Phys.* 2024. **26**: 11182.
33. Chen P.C. Crystal Sizes and Energy Gaps of Cerium Oxide Using Co-Precipitation Method. *Mater. Sci. Appl*. 2022. **13**: 213.
34. Matin A., Baig U., Gondal M.A., Akhtar S., Zubair S.M. Superhydrophobic and superoleophilic surfaces prepared by spray-coating of facile synthesized Cerium(IV) oxide nanoparticles for efficient oil/water separation. *Appl. Surf. Sci*. 2018. **462**: 95.
35. Hrynko A.M., Brichka A.V., Bakalinska O.M., Kartel M.T. Hydrogen peroxide decomposition by nanocomposites halloysite nanotubes/cerium oxide. *Him. Fiz. Tehnol. Poverhni*. 2025. **16**(3): 425.
36. Yokel R.A., Wohlleben W., Keller J.G., Hancock M.L., Unrine J.M., Butterfield D.A., Grulke E.A. The preparation temperature influences the physicochemical nature and activity of nanoceria. *Beilstein J. Nanotechnol.* 2021. **12**: 525.

Received 14.07.2025, accepted 04.12.2025